Phosphorylcholine-Based pH-Responsive Diblock Copolymer Micelles as Drug Delivery Vehicles: Light Scattering, Electron Microscopy, and Fluorescence Experiments

Cristiano Giacomelli, Lucile Le Men, and Redouane Borsali*

Laboratoire de Chimie des Polymères Organiques (LCPO)-ENSCPB, Université Bordeaux 1, 16 Av. Pey Berland, 33607 Pessac Cedex, France

Joséphine Lai-Kee-Him and Alain Brisson

Laboratoire d'Imagerie Moléculaire et Nano-Bio-Technologie (IECB), Université Bordeaux 1, 2 Rue Robert Escarpit, 33607 Pessac Cedex, France

Steven P. Armes*

Department of Chemistry, Dainton Building, Brook Hill, Sheffield, South Yorkshire, S3 7HF United Kingdom

Andrew L. Lewis

Biocompatibles UK Ltd, Chapman House, Farnham Business Park, Weydon Lane, Farnham, Surrey, GU9 8QL United Kingdom

Received November 22, 2005; Revised Manuscript Received January 13, 2006

The micellization behavior of a diblock copolymer comprising a highly hydrophilic and biocompatible poly(2-methacryloyloxyethyl phosphorylcholine) (PMPC) corona-forming block and a pH-sensitive poly(2-(diisopropylamino)ethyl methacrylate) (PDPA) core-forming block (PMPC-*b*-PDPA) has been studied by static and dynamic light scattering (SDLS), transmission electron microscopy (TEM), and potentiometry. Self-assembly of PMPC-*b*-PDPA copolymers with two different DPA volume fractions (ϕ_{DPA}) leads to narrowly distributed and structurally distinct spherical micelles, as evidenced by their molecular weight ($M_{w,mic}$), aggregation number (N_{agg}), hydrodynamic radius (R_H), corona width (W), and core radius (R_c). The excellent potential of these pH-responsive micelles as nanosized drug delivery vehicles was illustrated by the encapsulation of dipyridamole (DIP), a model hydrophobic drug that dissolves in acid solutions and becomes insoluble above pH 5.8, which is comparable to the pK_a of the PDPA block. The influence of micelle structure (namely $M_{w,mic}$, N_{agg}, R_H, W, and R_c) on drug loading content, drug loading efficiency, partition coefficient, and release kinetics was investigated and confirmed by fluorescence spectroscopy studies. The maximum dipyridamole loadings within $PMPC_{30}$-*b*-$PDPA_{30}$ (R_H = 14.0 nm; W = 4.8 nm; R_c = 9.2 nm) and $PMPC_{30}$-*b*-$PDPA_{60}$ (R_H = 27.1 nm; W = 11.0 nm; R_c = 16.1 nm) micelles were 7 and 12% w/w_p, respectively. This preferential solubilization of DIP into micelles formed by copolymer chains having longer core-forming blocks (i.e., possessing larger core volumes) reflects the larger partition coefficient (K_V) of DIP between the aqueous phase and $PMPC_{30}$-*b*-$PDPA_{60}$ micelles ($K_V = 5.7 \times 10^4$) compared to $PMPC_{30}$-*b*-$PDPA_{30}$ micelles ($K_V = 1.1 \times 10^4$). This enhanced ability of $PMPC_{30}$-*b*-$PDPA_{60}$ aggregates to entrap/stabilize small hydrophobic molecules also produces slower release kinetics. Rapid release can be triggered by lowering the pH to induce micellar dissociation.

1. Introduction

Over the past few decades, cellular membrane mimicking in relatively simple models has inspired many advances in the biomedical and nanotechnology fields, especially in terms of self-assembly processes involving phospholipid-like molecules.[1] These naturally occurring compounds usually comprise double hydrophobic tails and a polar headgroup, which in many cases contains the phosphorylcholine (PC) motif. On this basis, PC-based macromolecules of clinically proven biocompatibility have been successfully synthesized either by grafting PC moieties onto a reactive polymer backbone or by polymerizing PC-containing vinyl monomers such as 2-(methacryloyloxy)ethyl phosphorylcholine (MPC).[2,3] For example, Winnik et al.[4,5] reported the synthesis of hydrophobically modified PC-based polybetaines via reductive amination of phosphorylcholine glyceraldehyde by primary amine groups attached to the polymer. On the other hand, atom transfer radical polymerization (ATRP)[6] has been used by Armes and co-workers[7−10] to copolymerize MPC with various stimulus-responsive (pH, temperature, ionic strength) vinyl monomers to give a range of well-defined amphiphilic diblock and triblock copolymers.

One of the most interesting and fascinating properties of amphiphilic AB diblock copolymers is their ability to self-assemble into micelles (and other ordered structures such as lamellae, vesicles, etc.) if dissolved in a so-called "selective" solvent, i.e., a solvent that is thermodynamically good for one block and poor for the other.[11−17] Such micelles are characterized by their core−shell structure. In an aqueous environment, the hydrophobic blocks of the copolymer are segregated from

* To whom correspondence should be addressed. E-mail: borsali@enscpb.fr (R.B.); s.p.armes@sheffield.ac.uk (S.P.A.).

10.1021/bm0508921 CCC: $33.50
Published on Web 02/10/2006

Scheme 1. PMPC-*b*-PDPA Diblock Copolymer Structure and Its pH-Dependent Micellization Behavior

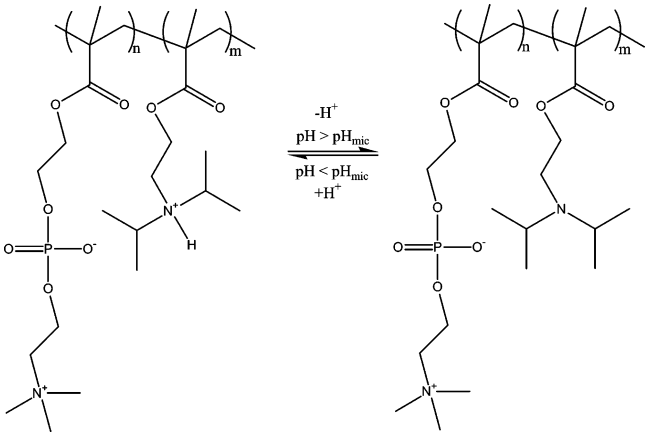

the aqueous exterior and form the inner core, whereas the hydrophilic blocks are located in the outer shell or corona.[17] Recently, copolymer micelles have been increasingly tested to be used as drug delivery vehicles due to the fact that the micelle cores can stabilize hydrophobic small molecules with otherwise limited water solubilities.[15,18] Advantages offered by block copolymer micelles for drug delivery applications include the following: (i) they can be designed to be either biocompatible and/or biodegradable; (ii) they are nanosized (10−100 nm diameter) and have a narrow size distribution, which allows intravenous injection; (iii) they are able to incorporate and release poorly water-soluble, hydrophobic, and/or highly toxic compounds; (iv) their use can minimize drug degradation and wastage, hence increasing bioavailability.[15,17,19] Furthermore, specific drug targeting through micellar drug delivery vehicles has been achieved by functionalizing the micelle surface with folic acid residues. This is because many malignant tissues consistently and uniformly express high levels of folate receptors, which are accessible via the bloodstream. Thus, drug-loaded folic acid-functionalized micelles can be used to selectively target cancer cells.[20] However, most pathological areas are characterized by local hyperthermia or acidosis, whereby micelles comprising stimuli-responsive (temperature or pH sensitive, respectively)[21] core-forming blocks can release their contents within those regions via triggered release.[22] Regarding pH-sensitive micelles, one of the major challenges has been the relatively narrow pH range over which the micellar carrier must both retain the drug over prolonged periods and then release it rapidly. In principle, the easiest way to achieve site-specific pH-triggered drug release into cells is by intravenous injection, assuming that the carriers are stable at physiological pH but release their payload once an acid pathological area is encountered (around pH 5.0−5.5). Such a narrow pH range can be obtained by appropriate selection of the alkyl substituents on the nitrogen atoms in poly(2-(dialkylamino)ethyl methacrylates).[21]

Herein we focus on diblock copolymers based on a highly hydrophilic corona-forming poly[2-(methacryloyloxy)ethyl phosphorylcholine] (PMPC) block and the pH-sensitive poly[2-(diisopropylamino)ethyl methacrylate] (PDPA) core-forming block (Scheme 1). Such PMPC-*b*-PDPA copolymers can be molecularly dissolved in dilute acidic solution, since the DPA block is protonated and hence hydrophilic under these conditions. On adjusting the copolymer solution to around pH 6−7, the PDPA becomes deprotonated and hence hydrophobic, leading to the formation of micelles with dehydrated PDPA cores and hydrated PMPC coronas as depicted in Figure 1. These

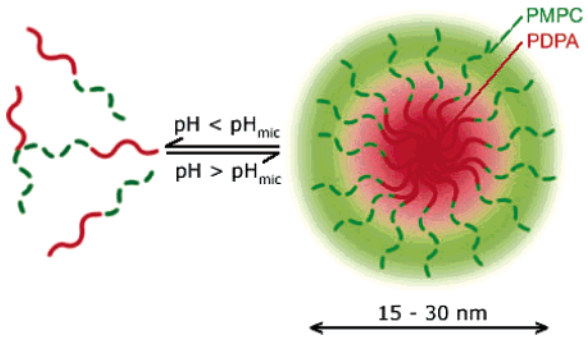

Figure 1. Micellization of PMPC-*b*-PDPA diblock copolymer as a function of the solution pH.

micelles have been loaded with both model hydrophobic molecules such as orange OT dye[23] and pyrene.[24] Pyrene fluorescence experiments indicate fairly similar partition coefficients (K_V) for PDPA−core micelles ($K_V = 1.1 \times 10^5$) and polystyrene−core micelles ($K_V = 1.9-2.4 \times 10^5$), suggesting that the ability of the PDPA cores to solubilize hydrophobic drugs is comparable to that of polystyrene-based micelles.[24]

The structure and dynamics of biocompatible block copolymer micelles as potential drug delivery vehicles are of considerable interest both before and after drug loading. Parameters such as micelle molar mass, aggregation number, hydrodynamic radius, corona width, and core radius have great implications for drug loading efficiency, partition coefficient, release kinetics, and micelle stability.[25]

The goal of this paper is therefore to gain further insight into the above physicochemical parameters associated with PMPC-*b*-PDPA micelles, which have not been extensively described to date. To this end, these micelles have been loaded with a poorly water-soluble model drug (dipyridamole, DIP), and various aspects of drug encapsulation such as the partition coefficient, drug loading content, drug loading efficiency, and the release kinetics were correlated with the micelle properties. DIP was chosen as a model drug because it had useful photophysical (fluorescence) properties and, last but not least, its aqueous solubility behavior closely mirrored that of the PDPA block.[26]

2. Experimental Section

Materials. The synthesis of the poly[2-(methacryloyloxy)ethyl phosphorylcholine]-*b*-poly[2-(diisopropylamino) ethyl methacrylate] (PMPC-*b*-PDPA) diblock copolymers was carried out via sequential monomer addition using ATRP as previously described elsewhere by Ma et al.[24] Briefly, an oligo(ethylene glycol)-based water-soluble initiator (OEGBr), a Cu(I)Br catalyst, and a 2,2′-bipyridine (bpy) ligand was used to polymerize MPC[2,3] (6.00 g, 20.2 mmol) in 10 mL of methanol using a [MPC]:[OEGBr]:[CuBr]:[bpy] relative molar ratio of either 30:1:1:2 or 60:1:1:2 under a nitrogen atmosphere at 20 °C. The polymerization was allowed to continue for approximately 2 h, at which point the monomer conversion was virtually complete. The required amount of DPA monomer was then added to this reaction solution and ^{1}H NMR used to monitor the reaction until monomer consumption was again complete (typically within 24 h at 20 °C). The reaction solutions were treated with silica gel to remove the ATRP catalyst, which resulted in the loss of around 10% of the diblock copolymer due to its adsorption onto the silica gel. Residual copper levels in the diblock copolymers were determined to be less than 2 ppm after this simple purification protocol. After solvent evaporation, the solid copolymers were washed with excess *n*-hexane to remove any traces of residual DPA monomer, redissolved in water, and then

Table 1. Characteristics of the Two PMPC-*b*-PDPA Copolymers Used to Prepared Phosphorylcholine-Based, pH-Responsive Micelles

copolymer architecture	M_n (g/mol)[b]	M_w/M_n[b]	ϕ_{DPA}[c]
$PMPC_{30}$-*b*-$PDPA_{30}$[a]	14 000	1.20	0.418
$PMPC_{30}$-*b*-$PDPA_{60}$[a]	21 000	1.27	0.590

[a] The subscripts indicate the mean degrees of polymerization (DP) of each block. [b] Data extracted from ref 22. [c] Volume fraction of DPA.

freeze-dried overnight. The characteristics of the resulting colorless copolymers are summarized in Table 1.

Sample Preparation. *Aqueous Micellar Solutions.* Dilute aqueous copolymer solutions ($C_p = 0.05-1.0$ mg/mL for $PMPC_{30}$-*b*-$PDPA_{60}$; $C_p = 0.5-4.0$ mg/mL for $PMPC_{30}$-*b*-$PDPA_{30}$) were made by molecularly dissolving the appropriate amount of copolymer in Milli-Q water that was adjusted to pH 3 using 1.0 mol dm^{-3} HCl. Where indicated, the respective ionic strength (I) of each solution was controlled by adding background electrolyte (either 0.05, 0.10, or 0.50 mol dm^{-3} NaCl). The samples were then stirred overnight to ensure complete copolymer dissolution. Afterward, micellization was induced by adjusting the solution pH to the desired value by addition of small amounts of 0.1 mol dm^{-3} NaOH. The contribution to the final I arising from the HCl and NaOH additions was neglected, as was the dilution due to added NaOH. Finally, the samples were filtered using 0.45 μm pore size nylon membrane filters in order to remove dust and any large, nonmicellar aggregates.

Drug-Loaded Micelles. Drug-loaded micelles were prepared using essentially the same procedure as described above, except that in this case appropriate amounts of DIP (Aldrich) (5, 10, 15, or 20% w/w_p; weight of DIP/weight of polymer) were dissolved at pH 3 along with the molecularly dissolved diblock copolymer. The unloaded DIP (yellow precipitate) was removed during the micelle filtration process.

Determination of the Critical Micelle Concentration (CMC). The critical micelle concentration (CMC) of the diblock copolymers was determined by fluorescence spectroscopy using pyrene (Py) as a probe.[27] Solutions containing 6.0×10^{-7} mol dm^{-3} Py (Aldrich) and molecularly dissolved copolymer ($C_p = 0.001-1.0$ mg/mL) were prepared by first adding known amounts of Py in acetone to empty volumetric flasks. After evaporation of the acetone, copolymer solutions at pH 3 were added to the same flasks, and stirred overnight to allow the resolubilization of Py. Subsequently, the solution pH was adjusted to 8−9 in order to induce micellization. The effect of increasing the copolymer concentration on the pyrene fluorescence profile was then assessed.

Partition Coefficient of DIP. The partition coefficient of DIP between the micelle core and the aqueous exterior environment was determined according to the methodology described by Tang et al.[26] Phosphate buffer solutions (0.50 mol dm^{-3} at pH 12.5) were prepared at a constant DIP content (5.0×10^{-6} mol dm^{-3}). Under these conditions DIP is fully soluble in water regardless of the solution pH, since its concentration is below its aqueous solubility constant (ca. 1.0×10^{-5} mol dm^{-3}).[26] Known amounts of molecularly dissolved copolymer (0.50 mL) were then added directly into the DIP buffer solution (2.0 mL) in the fluorescence cell.

Determination of Drug Loading in the Micelles. The loading efficiency of DIP incorporated into the PMPC-*b*-PDPA micelles was determined by fluorescence spectroscopy using the standard addition analytical method. Drug-loaded micelles were dissolved in citric acid/sodium citrate buffer at pH 3 to induce dissociation and to ensure a constant fluorescence quantum yield of DIP in aqueous solution. The fluorescence emission intensity at 490 nm ($\lambda_{exc} = 415$ nm) was measured as a function of known added aliquots (25, 50, 75, 100, 150, and 200 μL) of 3.8×10^{-3} mol dm^{-3} DIP. Linear fitting of experimental points generated straight lines, from which the "negative volume" of added DIP corresponding to zero fluorescence intensity was obtained, and accordingly the amount of DIP present in the original copolymer solution was calculated.

Release Kinetics. The release kinetics were assessed by placing a dialysis bag (MWCO 8000) containing 5 mL of the DIP-loaded micelles into a 5 L beaker filled with a phosphate buffer solution at pH 7.2, which was stirred constantly. At specific time intervals, 0.50 mL of the micelle solution in the dialysis bag was sampled and subsequently analyzed by fluorescence spectroscopy to determine the amount of probe release from the dialysis bag. The aliquot was then replaced into the dialysis bag without any dilution of the micelle solution.

Static and Dynamic Light Scattering Experiments. Static and dynamic light scattering (SDLS) measurements were performed using an ALV laser goniometer, which consists of a 22 mW HeNe linear polarized laser operating at a wavelength of 632.8 nm and an ALV-5000/EPP multiple τ digital correlator with 125 ns initial sampling time. Data were acquired using ALV Correlator Control software. Copolymer solutions were maintained at a constant temperature of 25.0 ± 0.1 °C in all experiments. The solutions were placed in 10 mm diameter glass cells. The minimum sample volume required for SDLS experiments was 1 mL. The accessible scattering angles range from 15° to 150°.

SLS measurements were carried out varying the scattering angle (θ) from 40 to 140° with a 5° stepwise increase. Toluene was used as a calibration standard. The weight-average molecular weight (M_w), z-average radius of gyration (R_g), and second virial coefficient (A_2) values were estimated from the relation

$$\frac{KC_p}{I(q)} = \frac{1}{M_w}\left(1 + \frac{1}{3}\langle R_g\rangle^2 q^2\right) + 2A_2C_p + ... \quad (1)$$

where $I(q)$ is the scattered intensity at a given q, $K = 4\pi^2n^2(dn/dC_p)^2//N_A\lambda^4$, with n being the refractive index of the solvent, dn/dC_p the refractive index increment against C_p, and N_A is Avogadro's number. The dn/dC_p value for PMPC-*b*-PDPA aqueous micellar solutions was 0.133 mL/g as determined using a differential refractometer built in our laboratory. By measuring $I(q)$ for a set of θ and C_p, values of M_w, R_g, and A_2 were estimated from typical Zimm plots.

DLS experiments were performed using the same apparatus; in this case, the counting time varied for each sample from 300 to 900 s. The relaxation time distributions, $A(\tau)$, were in the sequence obtained by CONTIN analysis[28] of the auto-correlation function, $C(q,t)$. The relaxation frequency, Γ ($\Gamma = \tau^{-1}$) is a function of the scattering angle.[29] The diffusion coefficient D is calculated from

$$D = \frac{\Gamma}{q^2}\Big|_{q\to 0} \quad (2)$$

where q is the wave vector defined as

$$q = \frac{4\pi n}{\lambda}\sin\left(\frac{\theta}{2}\right) \quad (3)$$

and λ is the wavelength of the incident laser beam (632.8 nm) and θ is the scattering angle. The translational diffusion coefficient at finite dilution (D_0) is calculated from

$$D = D_0(1 + k_dC_p) \quad (4)$$

where k_d is the concentration virial coefficient and C_p is the copolymer concentration. The hydrodynamic radius (R_H) is calculated from the Stokes−Einstein relation

$$R_H = \frac{k_BT}{6\pi\eta\Gamma}q^2 = \frac{k_BT}{6\pi\eta D_0} \quad (5)$$

where R_H is the hydrodynamic radius, k_B is Boltzmann constant, T is the temperature of the sample, and η is the viscosity of the medium.

Transmission Electron Microscopy (TEM). TEM images were recorded using a CM 120 Philips microscope operating at 120 kV, and equipped with a USC1000-SSCCD 2k × 2k Gatan camera. To prepare the TEM samples, 5 μL of an aqueous solution of block copolymer

micelles was dropped onto a carbon-coated copper grid, which was rendered hydrophilic by UV/ozone treatment. Excess micelle solution was gently removed using absorbent paper. Samples were then negatively stained by adding a 5 μL droplet of 2% phosphotungstic acid (PTA) at pH 7.5, and the excess solution was again removed prior to drying under ambient conditions. PTA was selected as a staining agent due to its chemical stability at pH 7.5, which is the solution pH for the formation of micellar aggregates in aqueous solution.

Potentiometric Titrations. PMPC-*b*-PDPA solutions at pH 3 were prepared as described above. Potentiometric titrations curves were obtained by monitoring the pH increase as a function of added 0.1 mol dm^{-3} NaOH (increments of 0.50 mL in a 10 mL diblock copolymer-containing solution). The pH measurements were performed using a Mettler Toledo pH meter coupled to an InLab 423 combined pH electrode, and titration curves in the pH range of 3 to 10 were recorded.

Fluorescence Experiments. Steady-state fluorescent spectra were measured using a FLX Safas Monaco spectrometer in the right-angle geometry (90° collector optics). For the fluorescence measurements, 2 mL of solution was placed in a 10-mm square quartz cell. All spectra were recorded from air-equilibrated solutions. For the fluorescence emission spectra, $\lambda_{ex} = 339$ nm when pyrene was used as probe, and $\lambda_{ex} = 415$ nm for dipyridamole. Spectra were accumulated with an integration time of 1 s per 0.5 nm.

3. Results and Discussion

3.1. Unloaded Micelles. *Dynamic Light Scattering (DLS).* On adjusting the solution pH of an aqueous copolymer solution containing molecularly dissolved chains (unimers) from pH 3 to around pH 6−7, the PDPA block becomes deprotonated and hence hydrophobic, leading to the formation of micelles with dehydrated PDPA cores and PMPC coronas,[24] according to Scheme 1 and Figure 1. However, the micelle molar mass, micelle aggregation number, hydrodynamic radius, corona width, and core radius of these micelles have still not been described. It is worth noting that the effect of different experimental conditions (especially ionic strength and temperature) during the micelle preparation procedure is of great importance in the current case due to the well-known conformational changes of polyelectrolyte chains that can be induced by salt addition. These aspects are of fundamental relevance when studying drug delivery systems since they may influence the circulation time, organ distribution, loading efficiency, and release kinetics.[15,17,19]

Figure 2 shows typical autocorrelation functions $C(q,t)$ and distributions of the relaxation times $A(t)$ at scattering angle of 90° as revealed by CONTIN analysis for 0.5 mg/mL solutions of (a) $PMPC_{30}$-*b*-$PDPA_{30}$ and (b) $PMPC_{30}$-*b*-$PDPA_{60}$ at pH 9 and an ionic strength close to zero (i.e., no added salt; a small amount of NaCl is nevertheless present due to the pH adjustment during the micelle preparation procedure). In both cases (Figure 2, panels A and B), narrow distributions of relaxation times were obtained, with a single dominant mode corresponding to the diffusive motion of the micelles in solution, whose characteristic hydrodynamic radius (R_H) was 15 nm for $PMPC_{30}$-*b*-$PDPA_{30}$ and 29 nm for $PMPC_{30}$-*b*-$PDPA_{60}$. These results are in very good agreement with other reports, which suggest that the length of the core-forming block dictates both the micelle dimensions and the micelle aggregation number and hence in turn the loading efficiency, drug release profile, partition coefficient, and bioavailability and biodistribution of the carrier system.

The insets in Figure 2 depict the typical q^2 dependence of the relaxation frequency (Γ) for diffusive scattering particles.[29] Thus, the R_H values discussed hereafter were calculated from

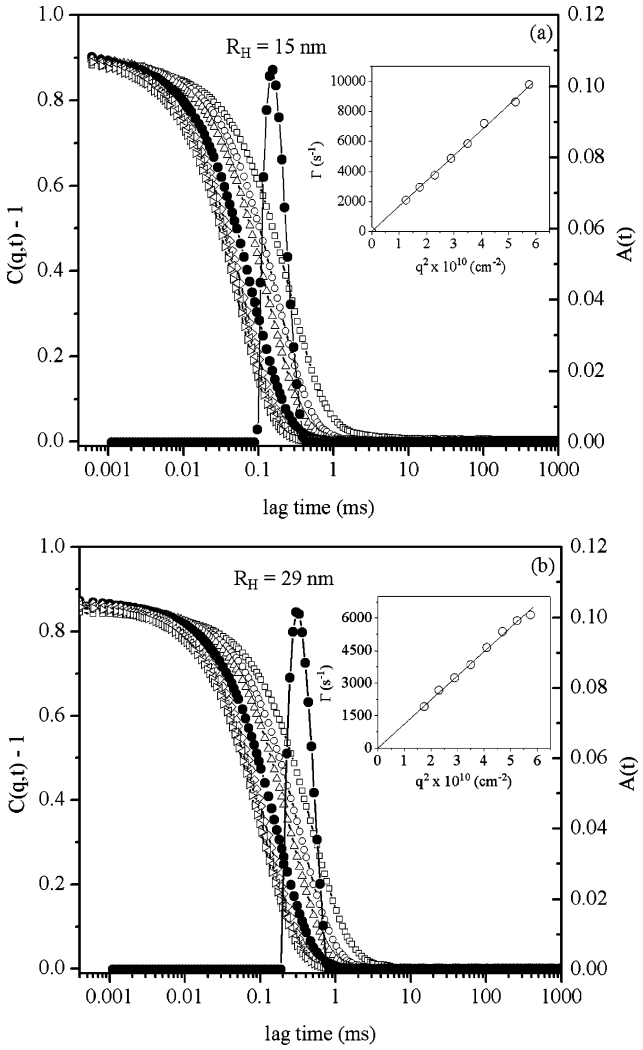

Figure 2. Autocorrelation functions $C(q,t)$ measured at scattering angles between 50° and 130°, and distributions of the relaxation times $A(t)$ at 90° as revealed by CONTIN analysis for 0.50 mg/mL solutions of (a) $PMPC_{30}$-*b*-$PDPA_{30}$ and (b) $PMPC_{30}$-*b*-$PDPA_{60}$ at pH 9 and zero added salt.

the Stokes−Einstein relation (eq 5) applied to relaxation time distributions that were recorded at a fixed scattering angle of 90°, although experimental data was also systematically recorded at different angles (data not shown).

The molecular features of PMPC-*b*-PDPA unimers at pH 3 are characteristic of a diblock linear polyelectrolyte (the PMPC chains have permanent zwitterionic character and the PDPA chains are cationic at this pH due to protonation). The aqueous solution behavior of polyelectrolytes has been extensively investigated, and certain features are now well established.[30−32] For example, it is known that the presence of charge on a polymer chain leads to its expansion with respect to the equivalent neutral polymer chain (or highly screened equivalent polyelectrolyte chain) and that lowering the ionic strength also leads to expansion of the polyelectrolyte coils. As the ionic strength decreases, the repulsion between polyelectrolyte chains increases, leading to a change in the second virial coefficient, A_2, and a reduction in light scattering intensity due to osmotic pressure.[30−32] Furthermore, the ionic strength also affects the critical degree of protonation of weak polyelectrolytes by stabilizing (screening) charged structures. As a result, the equilibrium constant shifts toward the formation of charged structures (see Scheme 1) and the critical micellization pH (pH_{mic}) increases. Thus, the weak polyelectrolyte nature of the

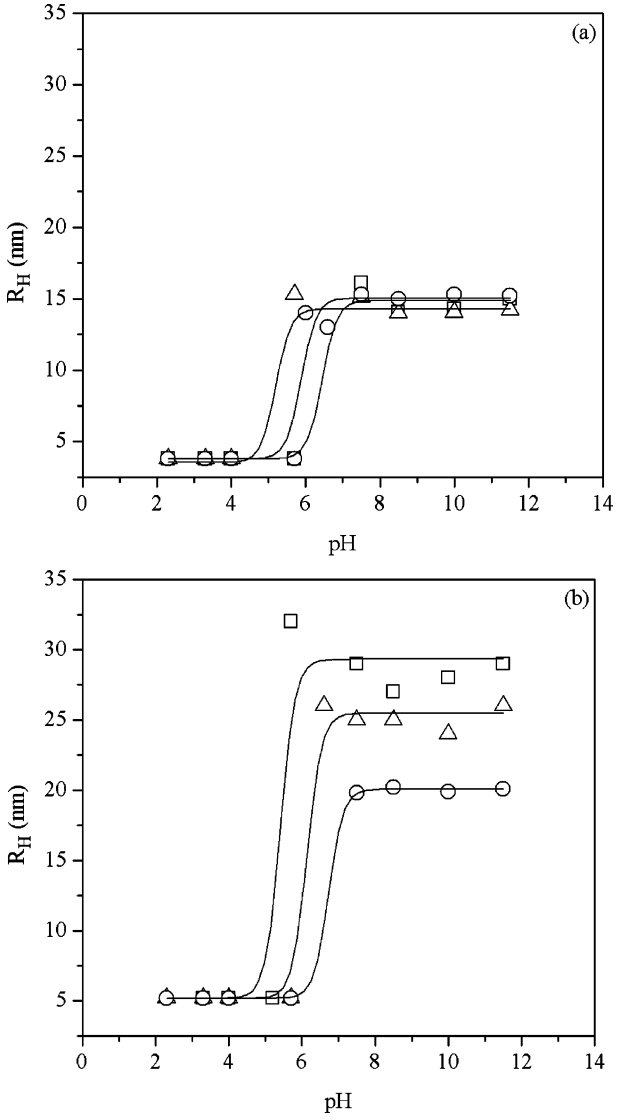

Figure 3. Variation of hydrodynamic radius (R_H) with solution pH at different ionic strengths ($I \sim$ zero, □; $I = 0.05$ mol dm^{-3}, △; $I = 0.1$ mol dm^{-3}, ○) (I) for (a) $PMPC_{30}$-*b*-$PDPA_{30}$ and (b) $PMPC_{30}$-*b*-$PDPA_{60}$ solutions.

PDPA block leads to a rich structural dependence of unimers and micelles on parameters such as ionic strength and pH for these copolymers.

The variation in hydrodynamic radius (R_H) as a function of the solution pH at different ionic strengths (I) is shown in Figure 3. Micellar aggregates formed by the pH-induced self-assembly of the copolymer with the shorter hydrophobic block ($PMPC_{30}$-*b*-$PDPA_{30}$; Figure 3A) presented virtually the same R_H values (ca. 15 nm) regardless of the ionic strength. In contrast, the R_H of the $PMPC_{30}$-*b*-$PDPA_{60}$ micelles (Figure 3B) decreased from 29 nm at $I \sim$ zero down to 19 nm at $I = 0.10$ mol dm^{-3}. However, in both cases, a shift in the critical micellization pH (pH_{mic}) occurred, which corresponds to the inflection point of the sigmoidal curves shown in Figure 3. The pH_{mic} was accurately determined from acid−base titration experiments (see below).

The effect of adding salt on the properties of micelles consisting of polyelectrolyte-type coronas (e.g., polystyrene-*b*-poly(acrylic acid) (PS-*b*-PAA) micelles) has been extensively studied by Eisenberg.[33] In general, charge screening leads to a reduction in the coil dimensions and, in turn, in the corona width. Conversely, the addition of salt after micellization does not affect the properties of $PMPC_{30}$-*b*-$PDPA_{60}$ micelles initially prepared at $I \sim 0$, whereas $PMPC_{30}$-*b*-$PDPA_{30}$ micelles are unaffected by ionic strength either before or after micellization. This unique behavior is most likely due to the polyzwitterionic nature of the PMPC block, which minimizes the effect of ionic strength on the coronal chains.

Hence, the differences in terms of size observed in Figure 3b ($PMPC_{30}$-*b*-$PDPA_{60}$ micelles) are attributable to changes in the micelle aggregation number (N_{agg}) and micelle molar mass ($M_{w,mic}$).

Static Light Scattering (SLS). The existence of a narrow, unimodal particle size distribution for the micelles formed by the $PMPC_{30}$-*b*-$PDPA_{30}$ (Figure 2a) and $PMPC_{30}$-*b*-$PDPA_{60}$ (Figure 2b) copolymers in aqueous solution allowed SLS measurements to be carried out with very good linear correlations between experimental data. Figure 4 shows typical Zimm plots obtained for $PMPC_{30}$-*b*-$PDPA_{30}$ (Figure 4A) and $PMPC_{30}$-*b*-$PDPA_{60}$ (Figure 4B) micelles investigated in this work, and the values of R_g, A_2, and $M_{w,mic}$ were calculated after double extrapolation to $C_p \rightarrow 0$ and $q \rightarrow 0$ (see Table 2). The micelle aggregation number (N_{agg}) was calculated using eq 6, where $M_{w,mic}$ is the micelle molar mass determined by SLS and $M_{w,unimers}$ is the molar mass of the respective individual diblock copolymer chains[34]

$$N_{agg} = \frac{M_{w,mic}}{M_{w,unimers}} \tag{6}$$

The micelle core radius, R_c, was derived from eq 7, where wtPDPA is the weight fraction of PDPA in the copolymer chain, N_A is the Avogadro number, d_{PDPA} is the solid-state density of PDPA, and Φ_{PDPA} is the volume fraction of PDPA in the micelle cores, which was assumed to be equal to unity in the case of PDPA in water (i.e., all of the PDPA chains are located within the micelle core).[34] Thus, the volume occupied by a single DPA repeat unit inside the micelle core (V_{DPA}) could be estimated from eq 8 on the basis of R_c values, where DP_{DPA} is the mean degree of polymerization of the PDPA block

$$R_c = \left(\frac{3M_{w,mic}wt_{PDPA}}{4\pi N_A d_{PDPA}\Phi_{PDPA}}\right)^{1/3} \tag{7}$$

$$V_{DPA} = \frac{4\pi R_c^{\,3}}{3N_{agg}DP_{DPA}} \tag{8}$$

The corona width (W) was calculated from relation 9

$$W = R_H - R_c \tag{9}$$

As can be deduced from Table 2, the micellar self-assembly of PMPC-*b*-PDPA block copolymers exhibiting different volume fractions of DPA (ϕ_{DPA}) clearly results in well-defined but

Table 2. Physicochemical Parameters of PMPC-*b*-PDPA Micelles Obtained by Combining SLS and DLS Results

copolymer	$M_{w,mic}$ (g/mol)	N_{agg}	A_2 (mol.L/g^2)	R_g (nm)	R_H (nm)	R_g/R_H	R_c (nm)	W (nm)	V_{DPA} (nm^3)/DPA
$PMPC_{30}$-*b*-$PDPA_{30}$	1.82×10^6	130	-1.33×10^{-8}	12.1	14.0	0.86	9.2	4.8	0.84
$PMPC_{30}$-*b*-$PDPA_{60}$	1.05×10^7	500	1.38×10^{-9}	25.0	27.1	0.92	16.1	11.0	0.57

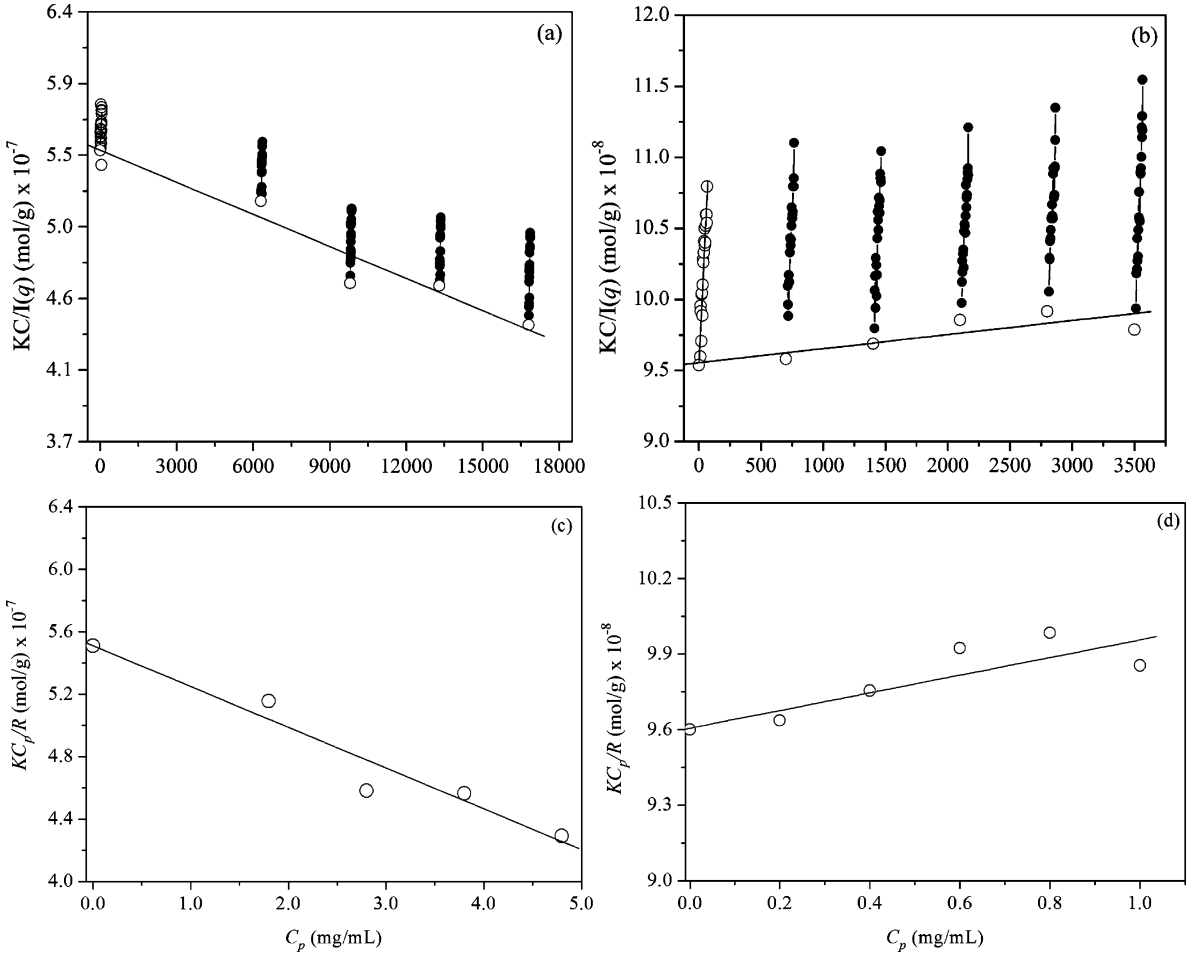

Figure 4. Typical Zimm plots (a,b) and C_p-dependence of the averaged light scattering intensity (c,d) obtained for aqueous micellar solutions of (a,c) $PMPC_{30}$-*b*-$PDPA_{30}$ (C_p = 1.8−4.8 mg/mL) and (b,d) $PMPC_{30}$-*b*-$PDPA_{60}$ (C_p = 0.2−1.0 mg/mL).

structurally distinct nano-objects. At low ionic strength (i.e. no added salt), the increase in the PDPA block length induces a significant increase in the micelle molar mass ($M_{w,mic}$) from 1.82 × 10^6 g/mol for $PMPC_{30}$-*b*-$PDPA_{30}$ to 1.05 × 10^7 g/mol for $PMPC_{30}$-*b*-$PDPA_{60}$. Such behavior reflects a substantial change in the respective N_{agg} from 130 to 500, respectively. Likewise, the R_g and R_H values increase significantly on increasing the mean degree of polymerization (DP) of the PDPA block (Table 2). The R_g/R_H ratio is often useful to characterize the shape of a molecular aggregate. The theoretical value of R_g/R_H for a homogeneous hard sphere is 0.779, and it increases substantially for less dense structures (R_g/R_H > 1 for vesicles and R_g/R_H > 1.5 for coils). The R_g/R_H values for $PMPC_{30}$-*b*-$PDPA_{30}$ and $PMPC_{30}$-*b*-$PDPA_{60}$ micelles are 0.86 and 0.92, respectively, suggesting the formation of approximately spherical micellar aggregates.[35]

Although the micelles studied in this work are spherical, their structures can vary significantly. Assuming that the terminal oligo(ethylene glycol)-based fragment (from the ATRP initiator) has typical C−C and C−O bond lengths of 1.53 and 1.43 Å, respectively, the corona width (W) value should be around 10 nm (the 2-bromoisobutyryl spacer at the block junction not included). Inspecting Table 2, the highly hydrophilic PMPC chains are clearly stretched into the solvent (W = 11.0 nm) in the case of $PMPC_{30}$-*b*-$PDPA_{60}$ micelles. In contrast, a coil-like conformation is most likely present for the $PMPC_{30}$-*b*-$PDPA_{30}$ micelles, since W is only 4.8 nm. Such variation in W values is accompanied by changes in the micelle core radius (R_c), which are obviously due to the increase in the length of the core-forming block. Considering that all of the PDPA chains are located inside the micelle core, it is also observed that the volume occupied by a single DPA repeat unit is smaller for more hydrophobic $PMPC_{30}$-*b*-$PDPA_{60}$ micelles (0.57 nm^3/monomer) than for $PMPC_{30}$-*b*-$PDPA_{30}$ micelles (0.84 nm^3/monomer) (Table 2). This suggests that the core is more compact in the former case. From a drug delivery point of view, these aspects clearly have implications for drug loading efficiency, drug release kinetics, and micelle stability.

The results in Figure 4, panels c and d, also indicate gradients of opposite sign for the two straight lines generated by extrapolating the $KC_p/I(q)|_{q\to 0}$ values to zero C_p, from which the second virial coefficients (A_2) were estimated as being −1.33 × 10^{-8} and +1.38 × 10^{-9} mol L/g^2 for $PMPC_{30}$-*b*-$PDPA_{30}$ and $PMPC_{30}$-*b*-$PDPA_{60}$ copolymers, respectively (see Table 2). The A_2 parameter depends on the interparticle interactions in solution. Whereas A_2 is zero for θ conditions, it is positive in the case of interparticle repulsions and negative in the case of attractive interactions. Unfortunately, it is not possible to draw reliable conclusions for these small A_2 values obtained for our systems. Besides, it is well-known that A_2 obtained by SLS for micelles may depend not only on the solvent nature but also on the surface tension at the core-corona interface.

Figure 5 shows a representative plot for the q^2 dependence of the averaged light scattering intensity for 0.1 mg/mL $PMPC_{30}$-*b*-$PDPA_{60}$ micellar solutions prepared at different ionic strengths (I). As $q \to 0$, eq 6 can be rewritten in the form of eq 10, which can be further simplified to eq 11 if the $2A_2C_p$ term is negligible. Assuming that A_2 is of the order of 10^{-8} mol L/g^2 (Table 2)

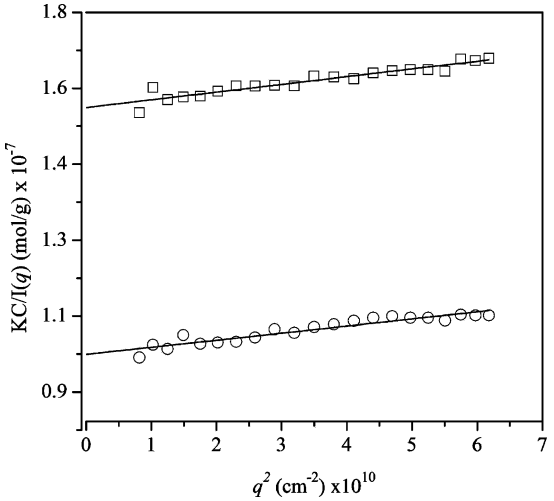

Figure 5. q^2 dependence of the averaged light scattering intensity for 0.10 mg/mL $PMPC_{30}$-*b*-$PDPA_{60}$ micellar solutions prepared at $I \sim$ zero (○) and $I = 0.10$ mol dm^{-3} (□).

regardless of the ionic strength, $2A_2C_p$ is approximately 2 orders of magnitude lower than $1/M_w$ ($\sim 10^{-7}$ mol/g) for $C_p = 0.1$ mg/mL

$$\frac{KC_p}{I(q)}|_{q\to 0} = \frac{1}{M_w} + 2A_2C_p \quad (10)$$

$$\frac{KC_p}{I(q)}|_{q\to 0;2A_2C_p\to 0} = \frac{1}{M_w} \quad (11)$$

$M_{w,mic}$ calculated from eq 11 is 1.0×10^7 g/mol at $I \sim 0$ and 6.3×10^6 g/mol at $I = 0.1$ mol dm^{-3}. Under these conditions, N_{agg} decreases from ca. 476 to ca. 300 with increasing I. Thus, it is obvious that varying the ionic strength primarily affects the polymer chain conformation prior to micellization, rather than electrostatic shielding effects between adjacent chains within the micellar corona. This interpretation seems reasonable since, below the critical micellization pH, the molecularly dissolved diblock copolymer comprises a polyzwitterionic-type PMPC block and a cationic PDPA block, which is certainly sensitive to the presence of added counterions.

Transmission Electron Microscopy (TEM). Figure 6 shows TEM images of negatively stained $PMPC_{30}$-*b*-$PDPA_{60}$ micelles prepared at (a) $I \sim 0$ and (b) $I = 0.1$ mol dm^{-3}. Surprisingly, in the present case, the micelle cores appear as gray-colored (low electron contrast) areas surrounded by a dark region that most likely corresponds to the micelle coronas. Such core−shell segregation is attributed to the selective staining of PMPC chains collapsed onto the hydrophilic carbon-coated copper grid.

In general, narrowly distributed nanosized spherical micelles are observed in Figure 6, panels a and b. The mean micelle radius in these micrographs (20−25 nm at $I \sim 0$ and 10−15 nm at $I = 0.1$ mol dm^{-3}) are evidently smaller than those determined by DLS measurements. This is in part due to micelle dehydration caused by solvent evaporation under the high vacuum conditions employed during TEM imaging. However, discrepancies are also expected because DLS reports an intensity-average diameter, whereas TEM reports a number-average diameter. Thus for a given size distribution of finite polydispersity, TEM images will always undersize relative to DLS data. Nevertheless, the images shown in Figure 6 corroborate the observed differences in $M_{w,mic}$, R_H, and N_{agg} revealed by DLS (Figure 3B) and SLS (Figure 5) experiments,

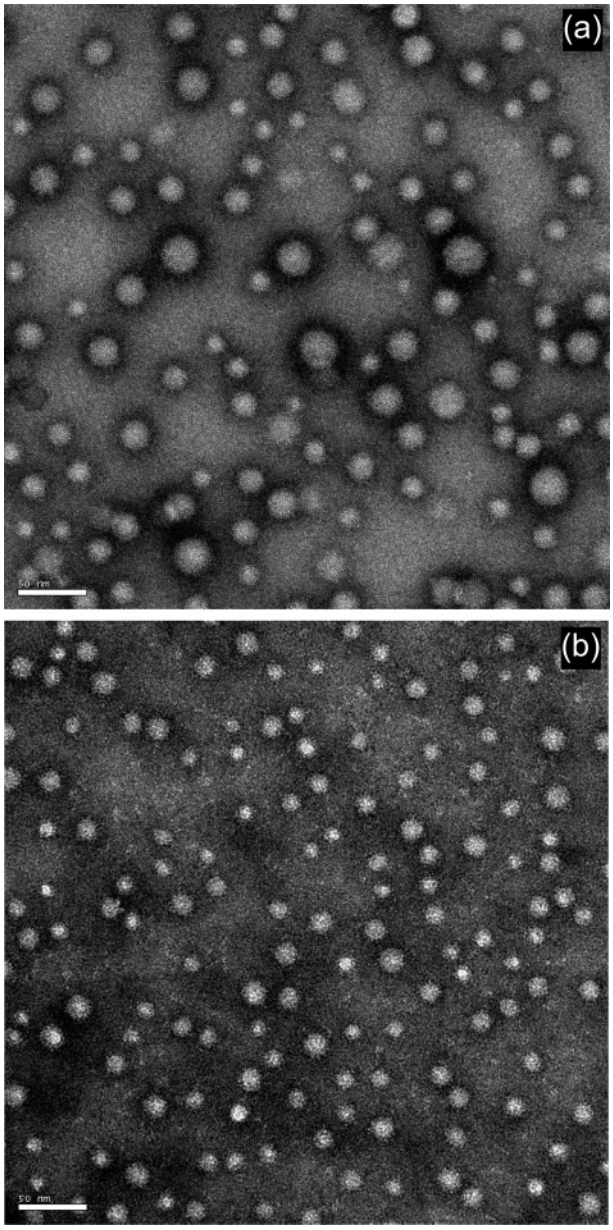

Figure 6. Transmission electron microscopy images of negatively stained $PMPC_{30}$-*b*-$PDPA_{60}$ micelles prepared at (a) $I \sim$ zero and (b) $I = 0.10$ mol dm^{-3}.

as deduced by comparing the mean micellar diameters in Figure 6, panels a and b.

The above comments also apply to micrographs taken for $PMPC_{30}$-*b*-$PDPA_{30}$ micelles (not shown) prepared using the same protocol, except that no noticeable size differences were observed on varying the ionic strength.

Potentiometric Titrations. Potentiometric measurements were performed in order to gain insight into the effect of ionic strength on the copolymer chains prior to micellization. The titration of PMPC-*b*-PDPA copolymer solutions can be modeled as the neutralization of a monobasic weak acid with a strong base, where the copolymer comprises DPA repeat units having an average pK_a.[36] Thus, the acid−base equilibrium can be represented as shown below, where HP^+ denotes the copolymer with positively charged (protonated) PDPA blocks, H^+ is the proton, and P is the neutralized (deprotonated) copolymer. The progressive addition of NaCl to such a system causes screening of the charges along the PDPA block, thus stabilizing the HP^+ species. Consequently, the equilibrium constant, K_a, which is defined

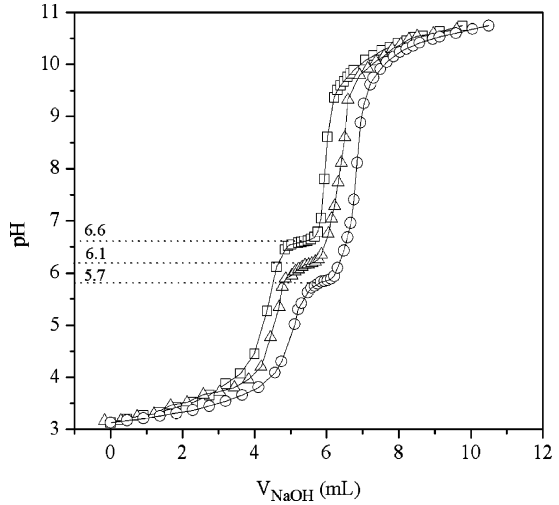

Figure 7. Potentiometric acid−base titration curves for 0.10 mg/mL $PMPC_{30}$-*b*-$PDPA_{60}$ solutions at different ionic strengths ($I \sim$ zero, □; $I = 0.05$ mol dm^{-3}, △; $I = 0.10$ mol dm^{-3}, ○).

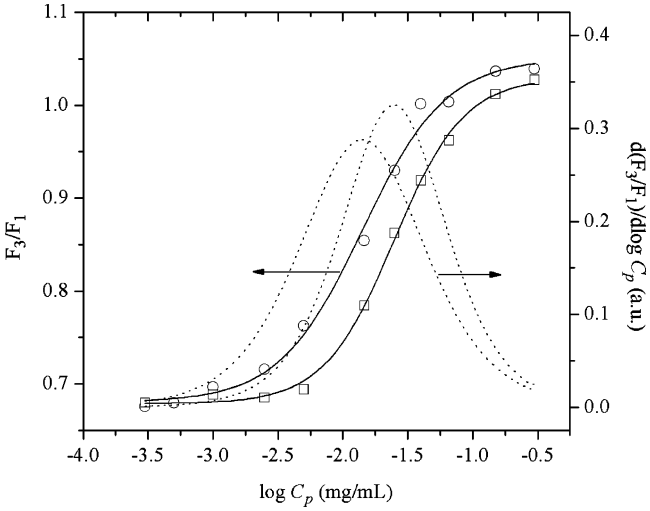

Figure 8. F_3/F_1 intensity ratios derived from pyrene emission spectra for $PMPC_{30}$-*b*-$PDPA_{30}$ (□) and $PMPC_{30}$-*b*-$PDPA_{60}$ (○) copolymer solutions as a function of C_p at pH 8, $\lambda_{exc} = 335$ nm. Dotted lines correspond to the first derivative of the solid lines.

by eq 12 and dictates the micellization thermodynamics, decreases due to the change in [HP^+] (square brackets stand for molar concentration). The average pK_a associated with the DPA groups in the PMPC-*b*-PDPA copolymer can be readily estimated from titration curves as the solution pH at 50% neutralization (i.e., where [HP^+] = [P]), whereupon eq 12 simplifies to eq 13

$$HP^+ \rightleftharpoons P + H^+$$

$$K_a = \frac{[P]\cdot[H^+]}{[HP^+]} \qquad (12)$$

$$K_a = [H^+] \therefore pH = pK_a = -\log(K_a) \qquad (13)$$

Figure 7 shows the potentiometric titration curves for 0.5 mg/mL $PMPC_{30}$-*b*-$PDPA_{60}$ copolymer solutions at different ionic strengths (no added salt; 0.05 mol dm^{-3} and 0.10 mol dm^{-3}). The small amounts of additional salt inevitably formed during titration were not taken into account. Starting from pH $\sim$ 3, the addition of small aliquots of NaOH increases the solution pH until a plateau is reached. In this buffering region, the added NaOH is consumed by the titration of the tertiary amine groups on the DPA repeat units, leading to micellization. After this process is complete, further addition of base merely elevates the solution pH. The average pK_a clearly depends on the salt concentration, varying from 5.7 (no added salt) up to 6.6 (I = 0.1 mol dm^{-3}) (Figure 7), as discussed above. These findings indicate that the critical micellization pH (pH_{mic}) of PMPC-*b*-PDPA copolymers can be controlled by adjusting the ionic strength. The same observations also apply to the $PMPC_{30}$-*b*-$PDPA_{30}$ copolymer (data not shown).

Fluorescence Experiments. It is well documented in the literature that the critical micelle concentration (CMC), which is the copolymer concentration below which only molecularly dissolved chains exist but above which both micelles and single chains are present simultaneously, is affected by the relative volume fraction (ϕ) of the core-forming block in a diblock copolymer. In general, reducing the core-forming block results in an increase in the CMC and a decrease in N_{agg} (this trend is observed in this work, see Table 2).[37] The CMC is of particular importance in the drug delivery field because it is related to micelle stability, and in turn to the partition coefficient, drug loading efficiency, and ultimately the drug release profile.[25] A micelle is thermodynamically stable with respect to dissociation provided that the copolymer concentration C_p is above the CMC. If $C_p <$ CMC, micelles may still be kinetically stable and survive for a given period of time, which will depend on the characteristics of the core-forming block (size, glass transition temperature, crystallinity).[15,38]

CMC values for the $PMPC_{30}$-*b*-$PDPA_{30}$ and $PMPC_{30}$-*b*-$PDPA_{60}$ copolymers were determined by fluorescence spectroscopy using pyrene. Pyrene has been widely used as a hydrophobic fluorescence probe to assess the polarity of various environments. Its fluorescence emission spectrum contains vibrational bands that are affected by the polarity of its surroundings. More specifically, changes in the relative intensities of the first (F_1 at 372 nm) and the third (F_3 at 383 nm) vibrational bands in the pyrene emission spectrum have proven to be reliable tools in examining the polarity of a microenvironment.[27] Thus, it is possible to follow the transfer of pyrene molecules from the polar aqueous phase to within the nonpolar micelle cores as C_p approaches the CMC and hence monitor the onset of micellization.

Figure 8 shows the F_3/F_1 intensity ratios derived from pyrene emission spectra recorded for $PMPC_{30}$-*b*-$PDPA_{30}$ and $PMPC_{30}$-*b*-$PDPA_{60}$ copolymer solutions as a function of C_p. At low C_p, where copolymer chains remain molecularly dissolved even though the solution pH is higher than pH_{mic}, the F_3/F_1 value is about 0.67. This value is slightly higher than that observed in pure water ($F_3/F_1 = 0.55$). As C_p increases, the F_3/F_1 ratio begins to increase as micellization commences, attaining a constant value ($F_3/F_1 \cong 1.00$) for $C_p >$ CMC. The CMC values for $PMPC_{30}$-*b*-$PDPA_{30}$ and $PMPC_{30}$-*b*-$PDPA_{60}$ were taken as the C_p at the inflection point (for the sake of clarity) of curves shown in Figure 8 and were found to be 0.025 and 0.014 mg/mL, respectively. These values are slightly lower than, for example, those reported for poly(ethylene oxide)-*b*-poly(propylene oxide)-*b*-poly(ethylene oxide) copolymers (0.03−0.3 mg/mL for PEO_{25}-*b*-PPO_{38}-*b*-PEO_{25} and PEO_{148}-*b*-PPO_{56}-*b*-PEO_{148})[39] but somewhat higher than those determined for poly(ethylene oxide)-*b*-polycaprolactone (0.0028 mg/mL for PEO_{45}-*b*-PCL_{21}).[15]

3.2. Dipyridamole (DIP) Loading. The partition coefficient, the drug loading content, drug loading efficiency, and the release

kinetics were evaluated and correlated with the micellar properties.

Encapsulation Method. Three different methods of drug encapsulation have been reported in the literature. The most common techniques are direct dissolution and dialysis, followed by a third approach consisting of a solvent-free strategy (which is pertinent to the present work). The method of choice depends largely on the solubilities of both the block copolymer and the drug in water. The direct dissolution method is normally employed when the copolymer is marginally soluble in water [e.g., poly(propylene oxide and poly(*N*-isopropylacrylamide)], whereas dialysis is usually preferred for poorly water-soluble copolymers such as polycaprolactone and poly(lactic acid).

Direct dissolution simply involves adding the copolymer and the drug to an aqueous medium, whereupon copolymer self-assembly, which may be induced by an external stimulus such as temperature variation, leads to drug entrapment. Dialysis is often used when micelles are to be formed from a copolymer that is not readily soluble in water. Both the copolymer and the drug are dissolved in a water-miscible organic solvent (i.e., a good solvent for both blocks such as THF, DMF, DMAc, or acetone). Subsequently, the copolymer/organic solvent/water mixture is dialyzed against water to remove the organic solvent. Due to the amphiphilic nature of the polymer chains, micellization is induced during dialysis, and the hydrophobic drug is consequently encapsulated.

The so-called solvent-free protocol for the preparation of drug-loaded block copolymer micelles in aqueous solution is a very attractive strategy, particularly if both the copolymer and the drug respond to the same external stimulus. In the present case, PMPC-*b*-PDPA and DIP are first molecularly dissolved in acidic solution (pH < pH_{mic}). Adjusting the solution pH to above the pH_{mic} leads to simultaneous micellization and drug solubilization.

The chemical structure of DIP contains both aromatic and aliphatic nitrogen atoms whose pK_a values are 5.7 and 12.5, respectively. The aqueous solubility constant (K_s) of DIP is strictly determined by its degree of protonation. Although completely water-soluble at pH < pK_{a1}, DIP precipitates from solution between pH 5.7 and 12.5 with a K_s of about 1.0×10^{-5} mol dm^{-3}. Above pH 12.5, the K_s is reduced by a factor of 5. It is noteworthy that the pK_{a1} of DIP (5.7) is very close to the average pK_a of 5.7−6.6 for the PDPA block (see Figure 7).

We elected to take advantage of the structure−solubility relationship of DIP and PMPC-*b*-PDPA by using the solvent-free method of drug entrapment. Figure 9 shows potentiometric titration curves of 0.5 mg/mL $PMPC_{30}$-*b*-$PDPA_{30}$ (a) and $PMPC_{30}$-*b*-$PDPA_{60}$ (b) in the presence of 0.1 mg/mL DIP. It is interesting to note that the presence of DIP does not change the profile of the titration curves, indicating the concomitant neutralization of both the copolymer and the drug. Evidently, neutralization of a DIP-containing solution extends the buffer plateau compared to DIP-free solutions, which suggests that the drug is precipitated and entrapped inside the hydrophobic micelle cores during the onset of micellization. Furthermore, the addition of DIP to copolymer solutions lowered the mean pK_a value of the PDPA block (dotted lines in Figure 9), thus favoring this drug/copolymer self-assembly process.

Partition Coefficient. The partition coefficient, K_V, of DIP between the aqueous exterior and the micellar core was determined as previously described.[26] For partitioning of a probe molecule between copolymer micelles and solution, with a partition coefficient K_V, it is possible to define the dependence of the maximum fluorescence emission with respect to the copolymer concentration, C_p, for a constant probe concentration as given in eq 14, where F_{min} is the fluorescence intensity in absence of micelles, F_{max} is the intensity when essentially all of the probe is located within the micelle cores (high C_p), F is the intensity measured at a copolymer concentration C_p, and ρ is the density of the micelle core (taken as 1.0 g/mL)

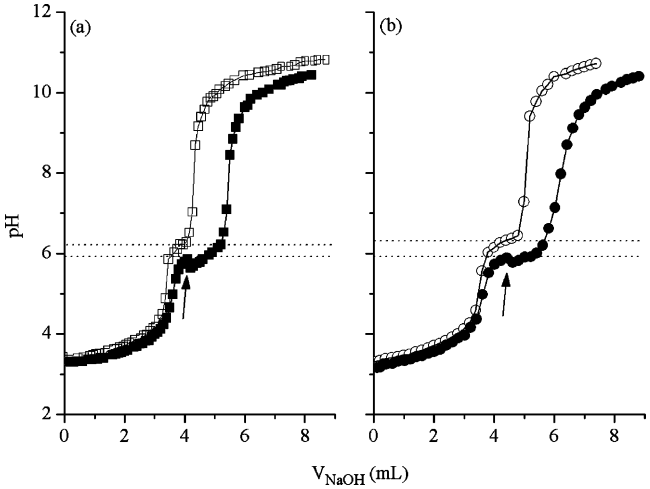

Figure 9. Potentiometric acid−base titration curves for 0.10 mg/mL solutions of (a) $PMPC_{30}$-*b*-$PDPA_{30}$ and (b) $PMPC_{30}$-*b*-$PDPA_{60}$ in the absence (○, □) and presence (●, ■) of DIP (titrant was 0.01 mol dm^{-3} NaOH).

$$\frac{1}{F - F_{min}} = \frac{1}{(F_{max} - F_{min})} + \frac{\rho}{K_V \phi_{DPA} C_p (F_{max} - F_{min})} \quad (14)$$

Thus, K_V can be determined from the slope and intercept of $1/(F - F_{min})$ against $1/C_p$ plot. Figure 10a shows the variation of DIP fluorescence spectra as a function of C_p. As expected, the intensity at the wavelength of maximum emission (λ_{max} = 490 nm) increases with C_p, generating good straight lines when plotted as $1/(F - F_{min})$ against $1/C_p$ (Figure 10b). The respective partition coefficients for $PMPC_{30}$-*b*-$PDPA_{30}$ and $PMPC_{30}$-*b*-$PDPA_{60}$ were 1.1×10^4 and 5.7×10^4, respectively. These values reveal strong partitioning of the hydrophobic small molecules into the micellar core, being comparable with those observed for pyrene/crew-cut poly(acrylic acid)-*b*-polystyrene ($K_V = 1.3 \times 10^5$)[40] and pyrene/poly(ethylene oxide)-*b*-polystyrene ($K_V = 2.0-4.0 \times 10^5$),[41] Cell Tracker CM-DiI/poly(ethylene oxide)-*b*-polycaprolactone ($K_V = 5.8 \times 10^3$)[38] systems, and relatively higher than for pyrene/poly(ethylene oxide)-*b*-polycaprolactone ($K_V = 1.0 \times 10^2$)[42] system. Using the same analytical approach, Tang et al.[26] found a K_p of $1.3-2.2 \times 10^4$ for the partitioning of DIP between micelles formed by poly(ethylene oxide)-*b*-poly(2-(dimethylamino)ethyl methacrylate)-*b*- poly(2-(diethylamino)ethyl methacrylate) and water.

The dependence of K_V on the volume fraction of DPA is expected, since the longer the core-forming block the greater the drug entrapment capacity.[15,25]

Drug Content and Drug Loading Efficiency. The amount of DIP incorporated into the PMPC-*b*-PDPA micelles, which was separated from free DIP by filtration (see the Experimental Section), was determined by fluorescence spectroscopy using the standard addition analytical method. This consists of dissolving drug-loaded micelles at a pH 3.0 buffer to induce micelle dissociation and ensure a constant fluorescence quantum yield of DIP in solution. After measuring the fluorescence emission intensity at 490 nm (λ_{exc} = 415 nm) of such a solution, known aliquots (25, 50, 75, 100, 150, and 200 μL) of a 3.8 ×

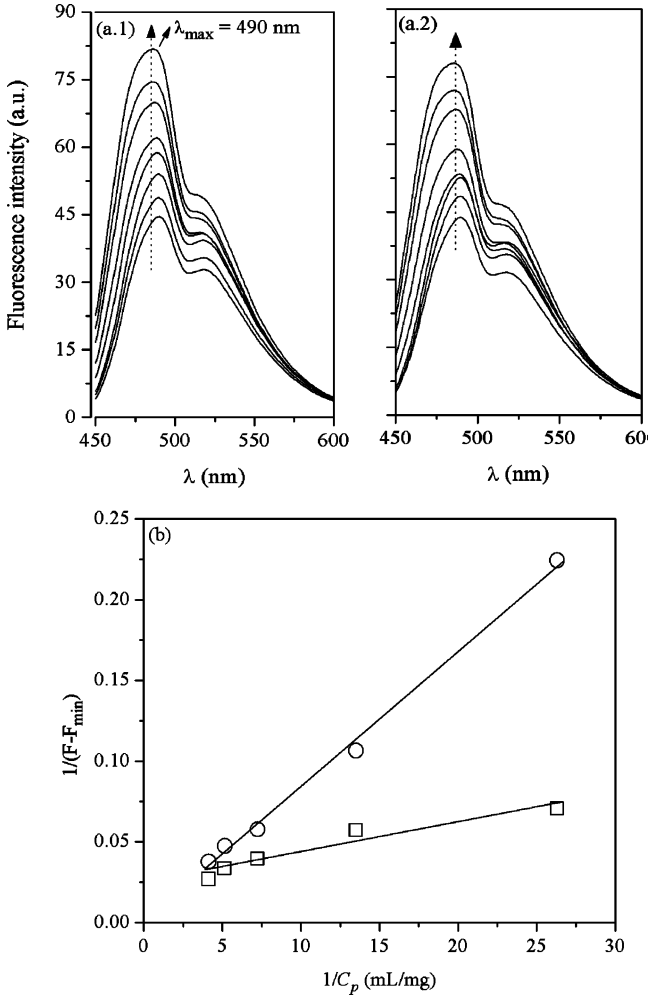

Figure 10. (a) DIP fluorescence spectra measured at C_p varying from 0.0 to 1.12 mg/mL, as indicated by the arrows, for PMPC$_{30}$-*b*-PDPA$_{30}$ (left) and PMPC$_{30}$-*b*-PDPA$_{60}$ (right); (b) determination of the partition coefficient of DIP between the aqueous phase and the micelle cores, as calculated from the data extracted from the spectra.

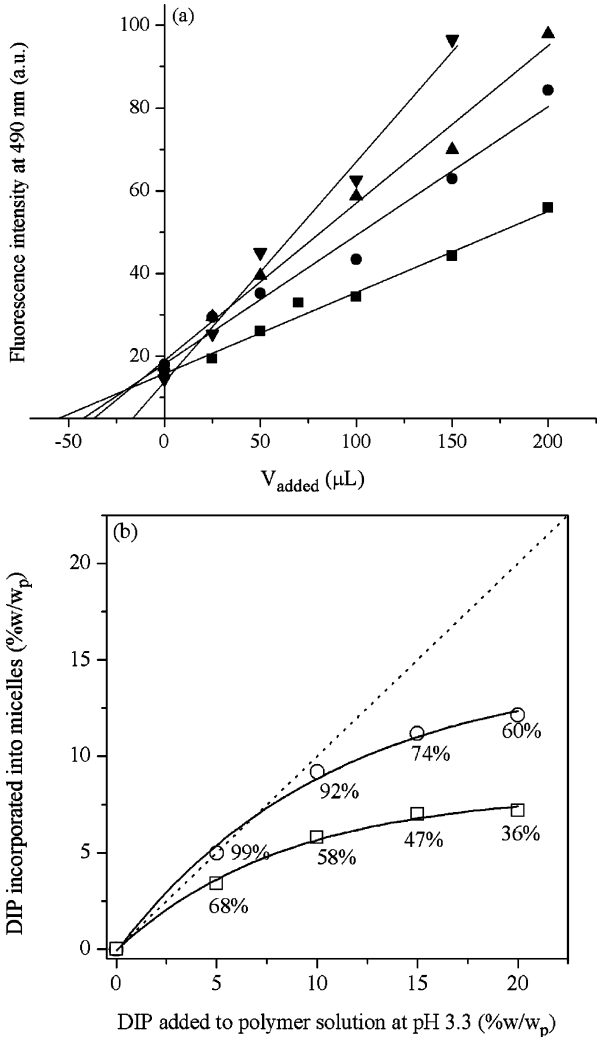

Figure 11. (a) Illustrative plot showing the DIP loadings of PMPC$_{30}$-*b*-PDPA$_{60}$ micelles prepared with varying quantities of added DIP [▼, 5; ▲, 10; ●, 15; and ■, 20% w/w$_p$ (weight/weight of polymer)] employing the standard addition method; (b) variation of drug content encapsulated within PMPC$_{30}$-*b*-PDPA$_{30}$ (□) and PMPC$_{30}$-*b*-PDPA$_{60}$ (○) micelles and the respective drug loading efficiencies as a function of added DIP.

10^{-3} mol dm^{-3} aqueous solution of DIP were added to the fluorescence cell, and a consequent increase in the emission intensity was recorded. Satisfactory linear fits ($r > 0.98$) of experimental data were obtained using this methodology, see Figure 11a. Thus, the "negative volume" of added DIP corresponding to a fluorescence intensity equal to zero was obtained, and accordingly, the amount of DIP present in the original solution ($[DIP]_{mic}$) was calculated using eq 15, where V_{DIP} is the "negative volume" illustrated in Figure 11a and V_{mic} is the volume of drug-containing micelle solution

$$[\mathrm{DIP}]_{mic}(\mathrm{mol/L}) = \frac{V_{DIP}(\mathrm{mL})3.8 \times 10^{-3}(\mathrm{mol/L})}{V_{mic}(\mathrm{mL})} \quad (15)$$

Figure 11b shows the variation of the encapsulated drug content and the respective drug loading efficiencies (defined by eq 16) as a function of the total mass of drug used. The dotted line denotes quantitative loading. In general, there is an increase in the encapsulated drug content as its amount in the initial solution increases, but eventually a maximum value is attained. The maximum DIP content loaded into the PMPC$_{30}$-*b*-PDPA$_{30}$ micelles is about 7% w/w$_p$ (corresponding to a loading efficiency of 36%) at an initial weight ratio of 20% w/w$_p$. However, this value increases up to 12% w/w$_p$ (60% loading efficiency) for micelles formed by the PMPC$_{30}$-*b*-PDPA$_{60}$ copolymer

$$\text{loading efficienty (\%)} = \frac{\text{mass of drug in micelles}}{\text{mass of drug used}} \times 100 \quad (16)$$

These results suggest that the capacity of PMPC-*b*-PDPA micellar aggregates to carry (deliver) dipyridamole molecules is strongly correlated to their structural properties. According to DLS and SLS experiments (see above), changing the volume fraction of DPA (ϕ_{DPA}) from 0.418 to 0.590 leads to an increase in the core volume from 3×10^3 nm^3 to 2×10^4 nm^3. The higher cargo space in the latter case is the main reason for the higher loading efficiency of PMPC$_{30}$-*b*-PDPA$_{60}$, along with nonnegligible contributions possibly arising from (i) the higher hydrophobicity of micelle cores formed by longer PDPA blocks, consequently enhancing interactions with the hydrophobic drug, and (ii) thicker corona acting as nanobarrier that can retard the diffusion of entrapped drug into aqueous media, where precipitation occurs.

Release Kinetics. The release of DIP encapsulated within PMPC-*b*-PDPA micelles is expected on lowering the solution

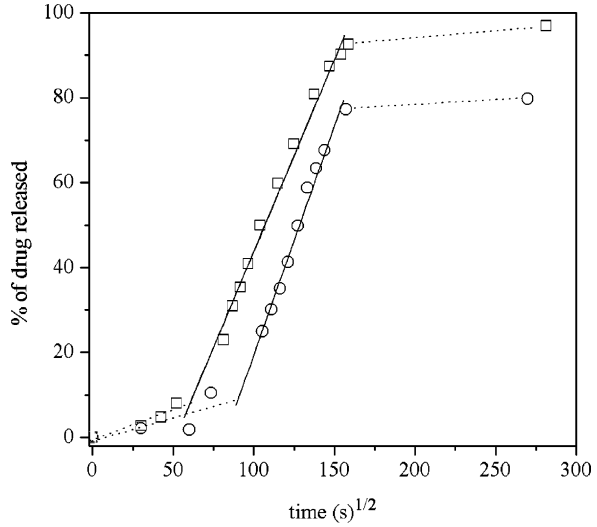

Figure 12. Percentage of DIP released as a function of the square root of time for 0.50 mg/mL $PMPC_{30}$-*b*-$PDPA_{30}$ (□) and $PMPC_{30}$-*b*-$PDPA_{60}$ (○) micelles prepared with initial DIP loadings of 7 and 12 w/w_p, respectively.

pH below pH_{mic}, since micellar dissociation occurs rapidly under these conditions. However, sustained release kinetics are normally sought in order to decrease the drug administration frequency. This process was assessed, and the results are summarized below.

Figure 12 shows the DIP quantity released from PMPC-*b*-PDPA micelles as a function of the square root of time. Regardless of the copolymer used, both profiles exhibit an induction period in which the released amount increases slowly and remains below to 10%. This time interval precedes the main release process and is attributed to drug diffusion inside the micelle, predominantly from the inner core toward the outer shell. Once the drug reaches the interface between the aqueous phase and the micelles, it is released at a constant rate (slope), accounting for a diffusion-controlled mechanism as proposed by Higuchi's model.[43] This is defined by eq 17, in which Q is the amount of drug released per area unit, C_0 is the initial drug content, and D is the apparent diffusion coefficient

$$Q = 2C_0\left(\frac{Dt}{\pi}\right)^{1/2} \tag{17}$$

According to the results shown in Figure 12, the amount of drug released within a 5 h period from 0.5 mg/mL $PMPC_{30}$-*b*-$PDPA_{30}$ (7% w/w_p DIP; Figure 11b) and $PMPC_{30}$-*b*-$PDPA_{60}$ (12% w/w_p DIP) micellar solutions was approximately 80 and 60%, respectively, with almost complete release being achieved after 20 h in the former case. On the other hand, the $PMPC_{30}$-*b*-$PDPA_{60}$ copolymer micelles retained around 20% of their original DIP content after 20 h, which is in agreement with their higher loading capacity and drug retention as the volume fraction of the core-forming block increases. Longer release periods have not been assessed at this time in this work.

The kinetics observed for DIP release from PMPC-*b*-PDPA micelles emphasizes the excellent potential of these phosphorylcholine-based pH-responsive copolymer micelles as drug delivery vehicles. Their capacity to retain and deliver DIP is comparable to pyrene- or Cell-Tracker DiI-loaded poly(ethylene oxide)-*b*-polycaprolactone micellar systems.[38]

4. Conclusions

PMPC-*b*-PDPA copolymers can be molecularly dissolved in dilute acid solution, since the PDPA block is protonated and hence hydrophilic under these conditions. On adjusting the copolymer solution to around pH 5−7, the PDPA blocks become deprotonated and hence hydrophobic, leading to the formation of micelles with dehydrated PDPA cores and PMPC coronas.

DLS studies confirmed that the micellar self-assembly of these PMPC-*b*-PDPA copolymers results in the formation of structurally distinct and narrowly distributed nano-spherical micelles. The characteristic hydrodynamic radius (R_H) is 15 nm for $PMPC_{30}$-*b*-$PDPA_{30}$ ($\phi_{DPA} = 0.418$) and 29 nm for $PMPC_{30}$-*b*-$PDPA_{60}$ ($\phi_{DPA} = 0.590$). On addition of salt prior to micellization, the $PMPC_{30}$-*b*-$PDPA_{60}$ micelle radius decreases from 29 nm (no added salt) down to 19 nm in the presence of 0.10 mol dm^{-3} NaCl, whereas essentially no salt effect was observed for the $PMPC_{30}$-*b*-$PDPA_{30}$ system. These differences correlate well with results obtained by SLS ($M_{w,mic}$, R_g, R_c, and W) and TEM studies.

Dipyridamole (DIP), a poorly water-soluble cardiovascular drug that dissolves in acid but is insoluble above pH 5.8, was loaded into these micelles using a solvent-free protocol (pH-induced micellization with simultaneous drug encapsulation). The influence of micellar properties on selected aspects of drug delivery such as drug loading content, drug loading efficiency, partition coefficient, and drug release kinetics was explored. The maximum drug loadings encapsulated into $PMPC_{30}$-*b*-$PDPA_{30}$ ($W = 4.8$ nm; $R_c = 9.2$ nm) and $PMPC_{30}$-*b*-$PDPA_{60}$ ($W = 11.0$ nm; $R_c = 16.1$ nm) micelles were 7 and 12%w/w_p, respectively. This preferential solubilization of DIP into micelles formed by copolymer chains having longer core-forming blocks (i.e., larger core volumes) reflects the higher partition coefficient (K_V) of DIP between the aqueous phase and $PMPC_{30}$-*b*-$PDPA_{60}$ micelles ($K_V = 5.7 \times 10^4$) compared to the $PMPC_{30}$-*b*-$PDPA_{30}$ micelles ($K_V = 1.1 \times 10^4$). Moreover, the $PMPC_{30}$-*b*-$PDPA_{60}$ micelles also produce significantly slower drug release kinetics, as expected.

Acknowledgment. R.B. acknowledges financial support from the CNRS, Université Bordeaux 1, Région Aquitaine and FEDER. C.G. acknowledges Coordenação de Aperfeiçoamento de Pessoal de Nível Superior (CAPES, Brazil) for the PhD fellowship. S.P.A. thanks Biocompatibles (Farnham, U.K.) for financial support, supply of the MPC monomer, and permission to publish these results. S.P.A. is the recipient of a five-year Royal Society/Wolfson Trust Research Merit Award.

References and Notes

(1) Richter, R. P.; Lai Kee Him, J.; Brisson, A. *Mater. Today* **2003**, *November*, 32−37.
(2) Kadoma, Y.; Nakabayashi, N.; Masuhara, E.; Yamauchi, J. *Kobunshi Ronbunshu* **1978**, *35*, 423−427.
(3) Ishihara, K.; Ueda, T.; Nakabayashi, N. *Polym. J.* **1990**, *22*, 355−360.
(4) Miyazawa, K.; Winnik, F. M. *J. Phys. Chem. B* **2003**, *107*, 10677−10682.
(5) Miyazawa, K.; Winnik, F. M. *Macromolecules* **2002**, *35*, 2440−2444.
(6) Matyjaszewski, K.; Davis, T. P. *Handbook of Radical Polymerization*; Wiley-Interscience: New York, 2002.
(7) Ma, I. Y.; Lobb, E. J.; Billingham, N. C.; Armes, S. P.; Lewis, A. L.; Lloyd, A. W.; Salvage, J. *Macromolecules* **2002**, *35*, 9306−9314.
(8) Li, Y.; Narain, R.; Ma, Y. H.; Lewis, A. L.; Armes, S. P. *Chem. Commun.* **2004**, 2746−2747.
(9) Lobb, E. J.; Ma, I.; Billingham, N. C.; Armes, S. P.; Lewis, A. L. *J. Am. Chem. Soc.* **2001**, *123*, 7913−7914.
(10) Lama, J. K. W.; Mab, Y.; Armes, S. P.; Lewis, A. L.; Baldwina, T.; Stolnika, S. *J. Controlled Release* **2004**, *100*, 293−312.
(11) Lodge, T. P.; Pudil, B.; Hanley, K. J. *Macromolecules* **2002**, *35*, 4707−4717.
(12) Lodge, T. P.; Bang, J.; Hanley, K. J.; Krocak, J.; Dahlquist, S.; Sujan, B.; Ott, J. *Langmuir* **2003**, *19*, 2103−2109.
(13) Discher, B. M.; Won, Y.-Y.; Ege, D. S.; Lee, J. C.-M.; Bates, F. S.; Discher, D. E.; Hammer, D. A. *Science* **1999**, *284*, 1143−1146.

(14) Discher, B. M.; Hammer, D. A.; Bates, F. S.; Discher, D. E. *Curr. Opin. Colloid Interface Sci.* **2000**, *5*, 125−131.
(15) Allen, C.; Maysinger, D.; Eisenberg, A. *Colloid Surf. B−Biointerfaces* **1999**, *16*, 3−27.
(16) Riess, G. *Prog. Polym. Sci.* **2003**, *28*, 1107−1170.
(17) Kataoka, K.; Harada, A.; Nagasaki, Y. *Adv. Drug Delivery Rev.* **2001**, *47*, 113−131.
(18) Francis, M.; Cristea, M.; Winnik, F. M. *Pure Appl. Chem.* **2004**, *76*, 1321−1335.
(19) Duncan, R. *Nat. Rev. Drug Discovery* **2003**, *2*, 347−360.
(20) Licciardi, M.; Tang, Y.; Billingham, N. C.; Armes, S. P.; Lewis, A. L. *Biomacromolecules* **2005**, *6*, 1085−1096.
(21) Gil, E. S.; Hudson, S. M. *Prog. Polym. Sci.* **2004**, *29*, 1173−1222.
(22) Torchilin, V. P. *Expert Opin. Ther. Patents* **2005**, *15*, 63−75.
(23) Salvage, J. P.; Rose, S. F.; Phillips, G. J.; Hanlon, G. W.; Lloyd, A. W.; Ma, I. Y.; Armes, S. P.; Billingham, N. C.; Lewis, A. L. *J. Controlled Release* **2005**, *104*, 259−270.
(24) Ma, Y. H.; Tang, Y. Q.; Billingham, N. C.; Armes, S. P.; Lewis, A. L.; Lloyd, A. W.; Salvage, J. P. *Macromolecules* **2003**, *36*, 3475−3484.
(25) Kwon, G. S.; Okano, T. *Adv. Drug Delivery Rev.* **1996**, *21*, 107−116.
(26) Tang, Y.; Liu, S. Y.; Armes, S. P.; Billingham, N. C. *Biomacromolecules* **2003**, *4*, 1636−1645.
(27) Kalyanasundaran, K.; Thomas, J. K. *J. Am. Chem. Soc.* **1977**, *99*, 2039−2044.
(28) Provencher, S. W. *Makromol. Chem.* **1979**, *180*, 201−209.
(29) Brown, W. *Dynamic Light Scattering. The Method and Some Applications*; Oxford University Press Inc.: New York, 1993.
(30) Borsali, R. In *Handbook of Polyelectrolytes and Their Applications*; Tripathy, S. K., Kumar, J., Nalwa, S., Eds.; American Scientific Publishers: Los Angeles, 2002; pp 249−265.
(31) Borsali, R. *Phys. Chem. Chem. Phys.* **1996**, *100*, 836−840.
(32) Borsali, R. *Macromol. Chem. Phys.* **1996**, *197*, 3947−3994.
(33) Zhang, L. F.; Eisenberg, A. *Macromolecules* **1996**, *29*, 8805−8815.
(34) Mountrichas, G.; Mpiri, M.; Pispas, S. *Macromolecules* **2005**, *38*, 940−947.
(35) Yusa, S. I.; Fukuda, K.; Yamamoto, T.; Ishihara, K.; Morishima, Y. *Biomacromolecules* **2005**, *6*, 663−670.
(36) Lee, A. S.; Gast, A. P.; Bütün, V.; Armes, S. P. *Macromolecules* **1999**, *32*, 4302−4310.
(37) Gadelle, F.; Koros, W. J.; Schechter, R. S. *Macromolecules* **1995**, *28*, 4883−4892.
(38) Soo, P. L.; Luo, L. B.; Maysinger, D.; Eisenberg, A. *Langmuir* **2002**, *18*, 9996−10004.
(39) Kabanov, A. V.; Nazarova, I. R.; Astafieva, I. V.; Batrakova, E. V.; Alakhov, V. Y.; Yaroslavov, A. A.; Kabanov, V. A. *Macromolecules* **1995**, *28*, 2303−2314.
(40) Zhao, J. X.; Allen, C.; Eisenberg, A. *Macromolecules* **1997**, *30*, 7143−7150.
(41) Wilhelm, M.; Zhao, C.-L.; Wang, Y.; Xu, R.; Winnik, M. A.; Mura, J.-L.; Riess, G.; Croucher, M. D. *Macromolecules* **1991**, *24*, 1033−1040.
(42) Allen, C.; Yu, Y.; Maysinger, D.; Eisenberg, A. *Bioconjugate Chem.* **1998**, *9*, 564−572.
(43) Higuchi, T. *J. Pharm. Sci.* **1961**, *50*, 874−875.

BM0508921